A cost-effective non-orthogonal 3D measurement system

Fengting Yang[1], Bin Wu[1,*], Wen Ding[1], You Xu[1], Ting Xue[2,*], Mohammed Farhan Ahmed[3], Jie Huang[3]

[1] State Key Laboratory of Precision Measuring Technology and Instruments, Tianjin University, Tianjin 300072, China;
[2] College of Electrical Engineering and Automation, Tianjin University, Tianjin Key Laboratory of Process Measurement and Control, Tianjin 300072, China;
[3] Department of Electrical and Computer Engineering, Missouri University of Science and Technology, Rolla 65409-0040, the United State;
* Correspondence: wubin@tju.edu.cn; Tel.: +86-136-4208-0876;
xueting@tju.edu.cn: Tel: +86-138-2036-3513;

Abstract: A novel cost-effective non-contact 3D measurement system is proposed in this paper, which consists of two rotary tables and one laser range finder. No orthogonal accuracy between the three axes (two rotation axes and the laser axis) is required, i.e. the three parts of the sensor unit (two rotary tables and the laser range finder) need not be assembled orthogonally, which lowers the barrier to manufacture it. Time for adjustment and recalibration with non-orthogonality is also saved, compared to traditional instrument. A computing algorithm is proposed for the system to measure all the points in the measurement space, and the experiments validate that the proposed system is able to deliver relevant performance for indoor and outdoor construction measurement.

Keywords: 3D measurement; non-orthogonal; large-scale metrology; cost-effective instrument

1. Introduction

3D measurement is an essential building block for manufacture and civil engineering to ensure the high quality of their products. By accurately measuring the 3D coordinates of the distributed points that designers are interested in, engineers will be able to determine whether the geometric shape of their product are consistent with the original designs, and constructors will be able to know where a certain structure has been correctly built. The 3D information provided by the 3D measurement system can also be used in robotic system to understand the world and interact with it (e.g. navigation, object recognition and manipulation).

Based on the scale of the zone that interested points distributed in (measurement space), we can roughly divide the 3D measurement tasks into: large scale measurement, regular scale measurement, and micro/nano scale measurement. While the measurement space in most regular scale measurement applications are from meters to sub-millimeters, it can vary from a few meters to hundreds of meters in large scale measurement [1] and can be hundreds of micrometers to sub-nanometers in micro/nano scale measurement [2]. The required measurement accuracy is also various among the applications. This paper mainly focuses on the large and regular scale measurement application, whose measurement space is from tens of centimeters to tens of meters and permissible error is in the millimeter level.

Theodolite, total station, and laser tracker are three commonly used, traditional measurement instruments in this field. Morris Driels and Uday Pathre used vision-based automatic theodolite to calibrate the motor parameters of a robot [3]; Panos Psimoulis and Stathis Stiros employed robotic total station for bridge deflection evaluation [4]; and Aguado S. compensated the volumetric error of machine tool with a laser tracker [5]. In addition, these kinds of equipment are wildly employed in large-scale industrial measurement [6-9]. Although different characteristics are shown in the instruments, one common thing they share is that they all rely on the orthogonality of sensor units

[10-12]. In the other words, they require the horizontal rotation axis, the vertical rotation axis and the laser beam or the optic axis to intersect at one spatial point and be perpendicular to each other. Higher the accuracy of these systems, better the orthogonality of their axes is fulfilled.

In practice, the main way to ensure the orthogonality of an instrument is to assemble it precisely, which is a time-consuming process, leading to a high economic cost. A new robotic total station with millimeter-level accuracy usually costs $20,000 to $29,000 [13], while the proposed system costs around $2,800, which can further be reduced in mass production. Determining the deviation with field procedures and compensating it mathematically is another way to ensure the orthogonality[14-16], but the effectiveness is often limited and it can only works when the included angle between the axes is slightly different from 90°.

To solve this conflict, Bin Wu et al introduced a new kind of measurement instrument called non-orthogonal shaft laser theodolite (N-Theodolite) [17, 18], and a novel calibration method for N-Theodolite was proposed recently [19]. The main idea of the N-Theodolite is to produce a high-precision measuring instrument that does not require orthogonality, the three axes of N-Theodolite can be abstracted as three skew lines. With the calibration and calculation method proposed in [19], a highly accurate measurement could be delivered through the intersection of the laser beams of two N-Theodolites.

However, in some cases like measuring the dynamic deformation of bridges [20] or the shape of a room [21], the required absolute accuracy (which is indicated by the deviation between the measurement result and the truth) is limited, while the convenience is highly of concern to the operator. For these applications, a novel cost-effective non-orthogonal 3D measurement system is presented in this paper. The sensor unit of the system could be simply assembled with a laser range finder (LRF) and two rotary tables, requiring no orthogonality (Figure 1 and Figure 2). All the points in the measurement space could be measured by a single sensor unit, leading to a convenient operation and concise computing strategy. No extrinsic parameter calibration process is required before the measurement (which is necessary for the N-Theodolite system), and only one sensor unit needs to be controlled during the measurement operation. The intrinsic parameters of the sensor unit can be calibrated with a single laser tracker or other alternative high precision 3D measurement devices, and only one-time calibration is needed for the system. As long as the assembly is firm enough, no further adjustment is required after calibration.

Several instruments with similar functions are available in the marketplace like Leica 3D-Disto [22]. However, to the best of our knowledge, they still rely on mechanical orthogonality to achieve high measurement accuracy. That means once non-orthogonality is observed, careful adjustment is needed, followed by recalibration. Sometimes, the process might be repeated to ensure the quality of the product, which costs lots of time even with modern manufacturing techniques, comparing to the one-time calibration of the proposed system without orthognality requirement. Waste rate related to orthogonal error decreases within the non-orthogonality framework at the same time, since no component of the sensor unit will be discarded during the manufacture as long as it can be assembled into a firm structure, i.e. this framework provides a high tolerance for the system to the flaw of its components.

The contribution of this paper is twofold:

1. We present a novel cost-effective non-orthogonal 3D measurement system that can be assembled with two rotary tables and one laser range finder with no orthogonal structure requirement;
2. We propose a calibration method which can be completed with a single laser tracker and a computing algorithm which can support the proposed non-orthogonal system to perform the 3D measurement.

This paper is organized as follows. Section 2 introduces the principle of the system including the design of the sensor unit and the structure of the system. The mathematic model, consisting of the calibration methods for intrinsic parameters, and the computing algorithm of the system, is

presented in Section 3. Section 4 describes the simulation and experiments of the novel system and a conclusion is drawn in Section 5.

2. The Principle of the Measuring System

2.1 The Design of the Sensor Unit

The proposed system is designed as a cost-effective device for large volume metrology. Two precise rotary tables are employed here, as well as a laser range finder (Leica Disto A6, measurement error 1.5mm/200m). These three parts are assembled manually without orthogonality requirement, i.e. the three axes of the sensor unit do not need to intersect at one point or be perpendicular to each other. Figure.1 shows the prototype of the sensor unit. The ball seat is glued for the calibration process using the laser tracker. The details of the calibration are stated in Section 3.

In convenience, we abstract the sensor unit to three skewed lines, called "Vertical axis", "Horizontal axis", and "Laser axis" respectively (Figure 2). When horizontal rotary table works, the horizontal axis and laser axis rotate around the vertical axis at the same time with the same angle, and when vertical rotary table works, laser axis rotates around the horizontal axis. According to the commands from the host computer, these two rotary tables can work together for a quick motion of the laser axis or work individually (one rotate while the other remains still). Every point in the measurement space can be pointed by the laser beam based on this rotating mechanism.

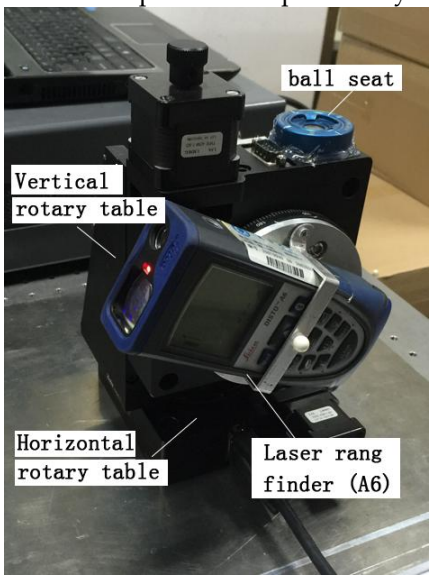

Figure 1. The prototype of the sensor unit

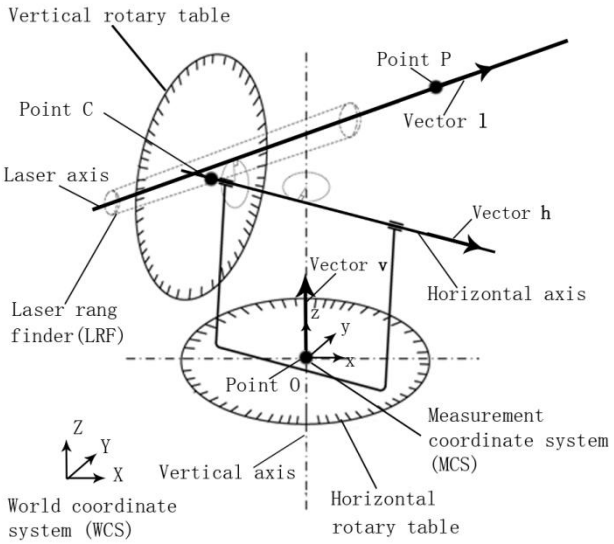

Figure 2. The abstract structure of the sensor unit

2.2 The Composition of Measurement System

The sensor unit can be controlled by a host computer via Bluetooth (for the Disto A6) and the servo cables (for the rotary tables). Once the object appears in measurement space, we can manually drive the sensor unit to aim at the target through the host computer. Based on the rotation angles and measured distance provided by the system, the coordinates of the target points can be determined. The operator can also program the measurement strategy to execute an automatic measurement using the proposed system.

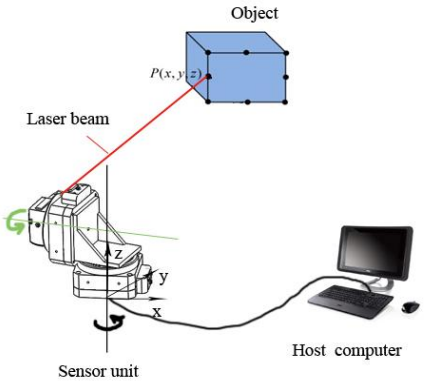

Figure 3. Schematic diagram of the measuring system

3. Mathematical Model of the Measuring System

3.1 Calibration Method for Intrinsic Parameters

As mentioned above, the structure of the sensor unit can be abstracted into three skew lines described by a normalized direction vector and a fixed point. A laser tracker is employed to calibrate these parameters—direction vectors and fixed points. It is worth to note the laser tracker can also be substituted by other highly precise measurement equipment like coordinate measurement machine (CMM) or theodolite based on the needs of the application.

The calibration process is as follows. First, a ball seat is glued to the surface of a "horizontal" circle plane with a ball placed on it during calibration (Figure 1). By rotating the horizontal rotary table degree-by-degree and measuring the center of the target ball in each position, we are able to get the normal vector and the rotation center of the rotary plane through circle fitting which indicates the position of the vertical axis. Second, glue the ball seat on the "vertical" circle plane and repeat the first step; the position of horizontal axis can be calibrated. Note the “horizontal/vertical circle plane” is not corresponding to the “horizontal/vertical rotary table”, instead the “horizontal/vertical circle plane” indicates a plane will stay “horizontally/vertically” and rotate around the vertical/horizontal axis. For example, the top plane of the vertical rotary table (where the ball seat is glued) is one horizontal circle plane and the side plane of the vertical rotary table (where the laser range finder is mounted) is a vertical circle plane. Third, we block the laser beam in different places (using a white board), and taking notes of the coordinate of the laser points measured by T-probe and its distance measured by the LRF. Figure 4 shows the detail implementation of this step. T-probe is a probe-like auxiliary tool which can work with the laser tracker to measure the coordinate of its pointing locations. The spatial position of laser beam could be determined by linear fitting. The flow chart of the calibration process is shown in Figure 4. All the elements shown in Figure 2, including three unit direction vectors (Vector **v**, Vector **h** and Vector **l**), three points (Point O, Point C and Point P) of the three axes, plus the initial horizontal and vertical angle of the sensor unit, the distance from original point of LRF to the chosen Point P at laser axis are called intrinsic parameters of the system.

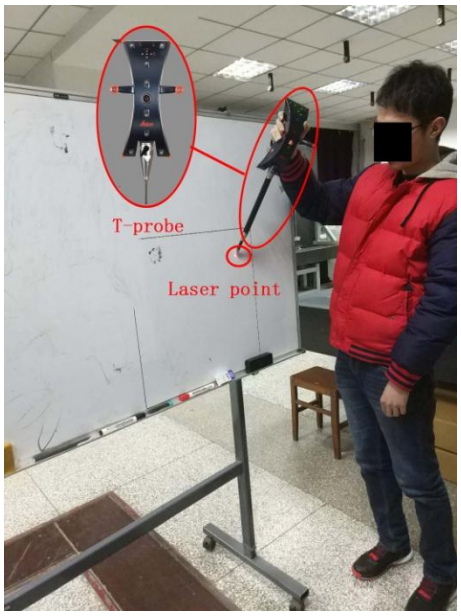

Figure 4. Implementation scenario of calibration step 3

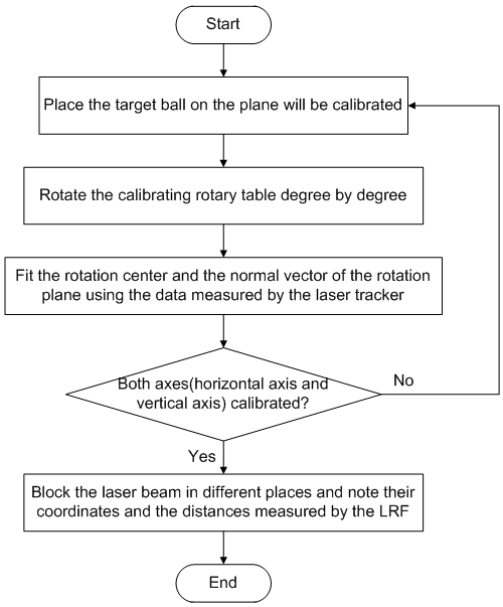

Figure 5. Flow chart of the calibration process

3.2 Computing Algorithm of the System

The measurement coordinate system of laser tracker is defined as the world coordinate system (WCS). As shown in Figure 2, the measurement coordinate system (MCS), which is the coordinate system of the sensor unit, is transformed from WCS. Translating WCS to the position where the origin of WCS coincides with the chosen Point O on vertical axis, and rotating WCS to parallel its z-axis to the vertical axis of sensor unit, we are able to establish the MCS. All the coordinates in this paper are referred to the MCS if no specific statement is made.

To calculate the coordinate of the target point, the dynamic position of Point P (the chosen point at laser axis) and the dynamic direction vector of laser axis have to be known. The motion of the laser axis can be broken down into two independent rotations, horizontal rotation (yaw) and vertical rotation (pitch), we focus on the horizontal rotation first.

$\mathbf{h}_{\text{original}}$ and $\mathbf{h}_{\text{dynamic}}$ are defined as the initial and dynamic homogeneous unit direction vectors of horizontal axis respectively, $\mathbf{h}_{\text{original}}, \mathbf{h}_{\text{dynamic}} \in \mathbf{R}^{4\times1}$, and $\mathbf{R}_{\text{hori}}$ is the rotation matrix between them. We have

$$\mathbf{h}_{dynamic} = \mathbf{R}_{hori}\mathbf{h}_{original} \tag{1}$$

Similarly, the dynamic position of chosen Point C has a similar equation

$$\mathbf{c}_{dynamic} = \mathbf{R}_{hori}\mathbf{c}_{original} \tag{2}$$

where $\mathbf{R}_{hori} = \begin{bmatrix} \cos(\theta) & \sin(\theta) & 0 & 0 \\ -\sin(\theta) & \cos(\theta) & 0 & 0 \\ 0 & 0 & 1 & 0 \\ 0 & 0 & 0 & 1 \end{bmatrix}$, as the default rotation of the horizontal rotary table is clockwise, θ is the horizontal rotation angle. $\mathbf{c}_{\text{original}}$ and $\mathbf{c}_{\text{dynamic}}$ are homogeneous vectors indicating the original and dynamic coordinates of Point C, $\mathbf{c}_{\text{original}}, \mathbf{c}_{\text{dynamic}} \in \mathbf{R}^{4\times1}$. The horizontal rotation of laser axis can be indicated by the same rotation matrix $\mathbf{R}_{\text{hori}}$, based on the structure of the sensor unit.

Turning to the vertical rotation, the dynamic homogeneous unit direction vectors of laser axis $\mathbf{l}_{\text{dynamic}}$ can be described by Eq.3,

$$\mathbf{l}_{\text{dynamic}} = [\mathbf{q} \circ [\mathbf{R}_{\text{hori}} \mathbf{l}_{\text{original}}]_{\text{q}} \circ \mathbf{q}^{-1}]_{\text{q}^{-1}} \tag{3}$$

where $\mathbf{l}_{\text{original}}$ is the original direction vector of the laser axis, $\mathbf{l}_{\text{dynamic}}, \mathbf{l}_{\text{original}} \in R^{4\times1}$; $\mathbf{q}$ is a quaternion indicating the φ-degree pitching rotation. According to the fundamental knowledge of quaternion [23], $\mathbf{q} = \cos(\varphi/2) + \vec{\text{h}}_{dynamic} \sin(\varphi/2)$, where $\vec{\text{h}}_{dynamic}$ is the non-homogeneous form of $\mathbf{h}_{\text{dynamic}}$, i.e. $\mathbf{h}_{\text{dynamic}} = (\vec{\text{h}}_{dynamic}, 1)^T$. Symbols "$[...]_{\text{q}}$" and "$[...]_{\text{q}^{-1}}$" indicate the transformation from homogeneous vector to quaternion and the inverse transform, respectively. Symbol " ∘ " means quaternion multiplication.

Since the relative position of Point C remains constant, the dynamic homogeneous coordinate vector $\mathbf{p}_{\text{dynamic}}$ shares the following expression

$$\mathbf{p}_{\text{dynamic}} = [\mathbf{q} \circ [\mathbf{R}_{\text{hori}} \mathbf{p}_{\text{original}} - \mathbf{c}_{\text{dynamic}}]_{\text{q}} \circ \mathbf{q}^{-1} + [\mathbf{c}_{\text{dynamic}}]]_{\text{q}^{-1}} \tag{4}$$

where $\mathbf{p}_{\text{original}}$ is the original homogeneous coordinate vector of the chosen Point P $\mathbf{p}_{\text{original}}, \mathbf{p}_{\text{dynamic}} \in R^{4\times1}$.

Assuming the measured distance between original point of LRF and Point P is k_1, and the distance from original point of LRF to target G is k_2, we have

$$\mathbf{t} = \mathbf{p}_{\text{dynamic}} + (k_2 - k_1)\mathbf{l}_{\text{dynamic}} \tag{5}$$

where $\mathbf{t}$ is the spatial homogeneous coordinate of the target point, $\mathbf{t} \in R^{4\times1}$. Thus the position of target points can be figured out by the rotary angle provided by the rotary tables and the measurement value of LRF, if the intrinsic parameters are calibrated precisely. Using the quaternion to calculate the measurement result speeds up the calculation process [24, 25], and the proposed algorithm can also be used by the traditional orthogonal instrument with orthogonal error to perform a high precision measurement .

4. Experimental Results and Analysis

4.1 Simulation of proposed measuring system

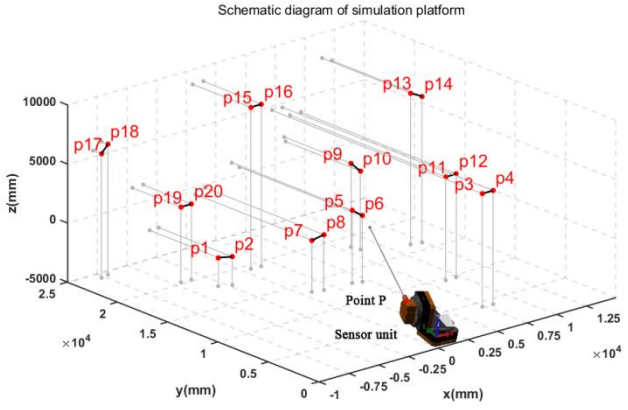

Figure.6 Schematic diagram of simulation platform

With the help of Solidworks[2012] and Matlab[R2014a], a simulation platform is set up for the proposed measuring system shown in Figure 5. Aiming at 20 different points in the measurement space, the stimulating system, whose intrinsic parameters are shown in Table 1, provides the measurement statistics including rotation angles as well as the measured distances between Point P and target points. The target coordinates can be determined by these measured data.

Table 1. Intrinsic parameters of the sensor unit from 3D models (mm)

Intrinsic parameters	Value
Vertical axis	Vector (0.000, 0.000,1.000) Point (0.000, 0.000,0.000)
Horizontal axis	Vector (0.985, 0.000, -0.174) Point (-226.374, 0.000, 872.388)
Sight axis	Vector (0.000, 1.000, 0.000) Point (-224.410, 952.486, 883.071)
Distance of Point P	0.000
Initial horizontal angle	0.000 degree
Initial vertical angle	0.000 degree

All the measured values shown in Table 1 are rounded to the nearest 3 decimal places to analyze the potential accuracy of the system in ideal condition. For the same purpose, the accuracy of rotary table is assumed to be 0.001°, and the distance measurement accuracy of the LRF is set to 0.01mm. So the potential performance of the proposed system with better devices can be evaluated. The comparison between the measurement values and the truth values offered by the Solidworks is presented in Table 2. The measurement space for simulation is 22000× 25000 ×12000mm.

Table 2. Comparison between measured value and truth value (mm)

No.	Measured Value	Truth Value	Distance k2(mm)	Deviation
1	(-3072.79, 18138.27, -2597.35)	(-3073.03, 18138.24, -2597.50)	18579.19	0.29
2	(-2292.96, 17689.39, -2598.44)	(-2292.94, 17689.39, -2598.46)	18025.65	0.03
3	(7248.40, 4088.38, 4603.82)	(7248.36, 4088.48, 4603.91)	9510.54	0.13
4	(8148.39, 4088.41, 4603.93)	(8148.36, 4088.48, 4603.91)	10213.1	0.08
5	(3842.69, 13000.40, 1162.47)	(3842.55, 13000.47, 1162.41)	13606.2	0.17
6	(4498.04, 12768.57, 590.83)	(4497.94, 12768.61, 590.83)	13550.57	0.11
7	(776.35, 13393.10, -638.18)	(776.24, 13393.13, -638.21)	13430.78	0.12
8	(1585.03, 13162.95, -317.12)	(1584.87, 13162.99, -317.03)	13261.85	0.20
9	(8293.84, 18359.69, 2045.47)	(8293.74, 18359.75, 2045.58)	20249.71	0.17
10	(8385.41, 17556.16, 1650.62)	(8385.25, 17556.28, 1650.53)	19525.87	0.22
11	(8782.85, 9534.82, 3739.37)	(8782.74, 9534.92, 3739.27)	13491.97	0.18
12	(9682.87, 9534.84, 3739.30)	(9682.74, 9534.92, 3739.27)	14094.41	0.16
13	(11494.87, 16219.56, 7809.39)	(11494.91, 16219.47, 7809.52)	21358.67	0.17
14	(12263.95, 15999.18, 7396.68)	(12263.81, 15999.28, 7396.82)	21473.03	0.23
15	(589.78, 19258.16, 8704.92)	(589.55, 19258.24, 8704.84)	21142.41	0.25
16	(1489.77, 19258.15, 8704.89)	(1489.55, 19258.24, 8704.84)	21186.62	0.25
17	(-7827.62, 24181.98, 5512.66)	(-7827.82,24181.96, 5512.59)	26008.28	0.21
18	(-7126.90, 24353.25, 6050.95)	(-7127.09,24353.21, 6050.79)	26086.13	0.25

19	(-4502.55, 20197.91, 1399.99)	(-4502.76, 20197.82, 1400.09)	20740.95	0.25
20	(-3602.54, 20197.86, 1400.16)	(-3602.76,20197.82, 1400.09)	20564.34	0.23

The simulation results generated under ideal circumstances shows that the measurement errors increase slightly as the distance of the test points from the chosen Point P increases. The value of the average relative error (absolute error divided by the distance from Point P) is 1.12×10^{-5} with a standard deviation of 7.89×10^{-7}. In absolute term, the average measurement error of the proposed system with simulated data is 0.18±0.11mm at an around 17m average distance, showing great potential to deliver a highly precise measurement.

4.2 Indoor experiment of the proposed system

In the indoor experiment, we employed a laser tracker to calibrate the intrinsic parameters of the sensor unit firstly (shown in Table 3). All the values were rounded to 3 decimal places, in agreement with calibration accuracy. Several paper targets were pasted on a target board which can be moved to different places in the measurement space (Figure 7). Both instruments were employed to measure the same points, and the distances between each couple measured by both approaches were compared. The comparison results are shown in Table 4, and the distribution of the target points is shown in Figure 8.

Table 3. Intrinsic parameters of the proposed system (mm)

Intrinsic Parameters		Value
Vertical axis	Vector	(0.000, 0.000, 1.000)
	Point	(0.000, 0.000, 0.000)
Horizontal axis	Vector	(0.810, 0.587, -0.000)
	Point	(-95.055, -74.808, -101.507)
Sight axis	Vector	(-0.577, 0.814, 0.061)
	Point	(-4090.509, 5575.764, 327.220)
Distance of Point P		6984.056
Initial horizontal angle		0.000 degree
Initial vertical angle		40.000 degree

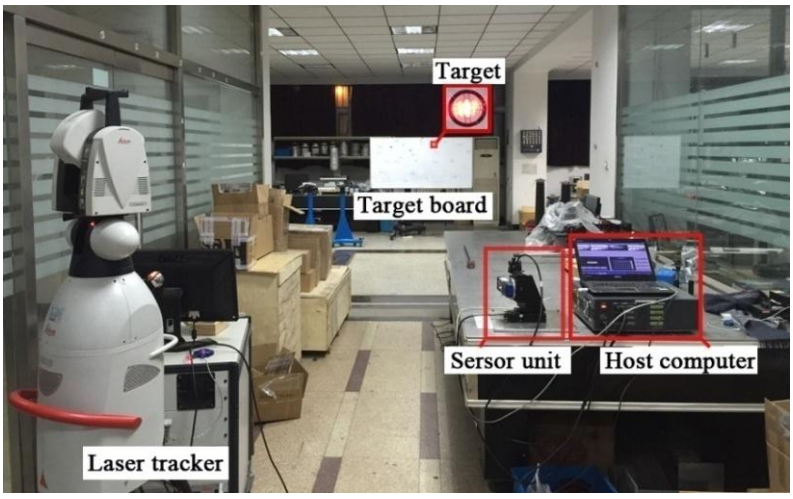

Figure.7 Indoor experiment condition

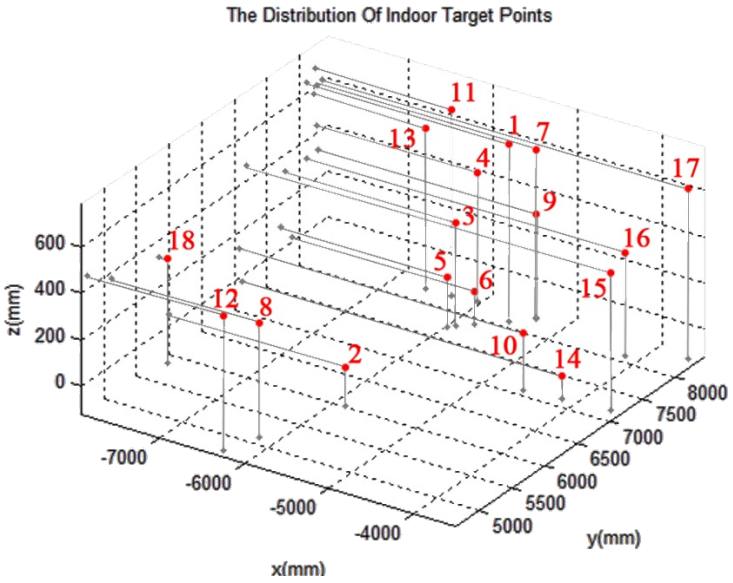

Figure.8 The distribution of indoor target points

Table 4. Comparison between two approaches of indoor experiment

No.	Horizontal angle Θ (°)	Vertical angle ϕ (°)	Distance K_2 (mm)	Proposed Approach (mm)	Laser Tracker Approach (mm)	Deviation (mm)
1	1.64	40.84	9892	2206.6	2207.4	-0.8
2	-8.22	37.48	8443			
3	-1.33	38.99	9833	509.4	508.9	0.5
4	-0.24	39.47	10296			
5	-1.78	37.63	9818	262.6	261.9	0.7
6	-0.31	37.18	9832			
7	3.10	40.59	9926	3276.8	3276.0	0.8
8	-14.30	39.85	8098			
9	3.10	38.92	9942	1454.3	1454.7	-0.4
10	3.16	38.00	8495			
11	-1.57	40.80	10463	3490.2	3490.0	0.2
12	-17.00	40.51	7986			
13	-2.90	40.14	10627	2755.6	2754.9	0.7
14	5.83	37.00	8304			
15	8.80	39.11	9181	1075.8	1075.7	0.1
16	9.34	40.51	8128			
17	12.70	40.98	9174	4931.4	4928.9	2.5
18	-17.30	38.98	9849			

Limited by the accuracy of the rotary tables (0.005°), the laser range finder (±1.5mm/200m), and the aiming accuracy, the measurement accuracy of the prototype does not match the quality of the simulation results. We round all the measurement result to the 1 decimal place to be corresponding to the measurement accuracy of the LRF. The distance range of the indoor measurement is from 8m to 10.6m, and the mean of the absolute value of the deviation is 0.7mm. The worst case shows a 0.25mm deviation with an around 4.9-meter target length in 9m measuring

distance. It is consistent with the uncertainty analysis in [26], and it is still able to meet the need of the most indoor architecture measurement application [21, 27].

4.3 Outdoor experiment of proposed system

In the outdoor experiment, we pasted paper targets on a building and measure the coordinate of each point (Figure 9). The distances between different points measured by the metric ruler (0.5mm/10m) and the proposed system are compared. The distribution of the segments and points are shown in Figure10. Table 5 shows the measuring angles and the measured coordinates of the 14 points, and Table 6 presents the comparison results.

Table 5. Measuring values of outdoor experiment

No.	horizontal angle Θ (°)	vertical angle ϕ (°)	Distance K2 (mm)	Measured coordinate (mm)
1	30.50	53.11	13660	(-1202.5, 12978.5, 3795.6)
2	20.57	54.61	12603	(-3139.0, 11502.5, 3806.8)
3	19.57	54.61	12668	(-3356.0, 11505.4, 3827.0)
4	18.05	58.35	14588	(-4100.9, 12846.2 5315.7)
5	30.08	68.35	15307	(-1270.7, 12887.4, 7955.5)
6	21.07	70.65	14509	(-3026.5, 11566.5, 8020.7)
7	17.27	71.45	16398	(-4225.8, 12706.0, 9269.4)
8	17.08	53.36	14062	(-4296.5, 12694.3, 3969.2)
9	25.08	52.86	12931	(-2302.1, 12135.2, 3533.2)
10	24.08	69.36	14631	(-2471.7, 11985.9, 7815.6)
11	18.08	68.16	15315	(-3932.6, 12373.5, 7916.7)
12	17.48	52.96	13894	(-4167.4, 12597.2, 3827.8)
13	19.48	52.96	12634	(-3395.9, 11572.5, 3470.5)
14	17.88	68.16	15458	(-4012.0, 12475.9, 7991.7)

Table 6. Comparison between two approaches of outdoor experiment

Segment Number	Proposed Approach (mm)	Ruler Approach (mm)	Deviation (mm)
1	2435.0	2435.0	0.0
2	2137.5	2135.5	2.0
3	2198.2	2196.0	2.2
4	5300.7	5300.0	0.7
5	4288.4	4286.5	1.9
6	4101.7	4101.0	0.7
7	4651.6	4651.0	0.6
8	1423.3	1426.5	3.2
9	149.8	148.0	1.8
10	1331.5	1335.0	3.5

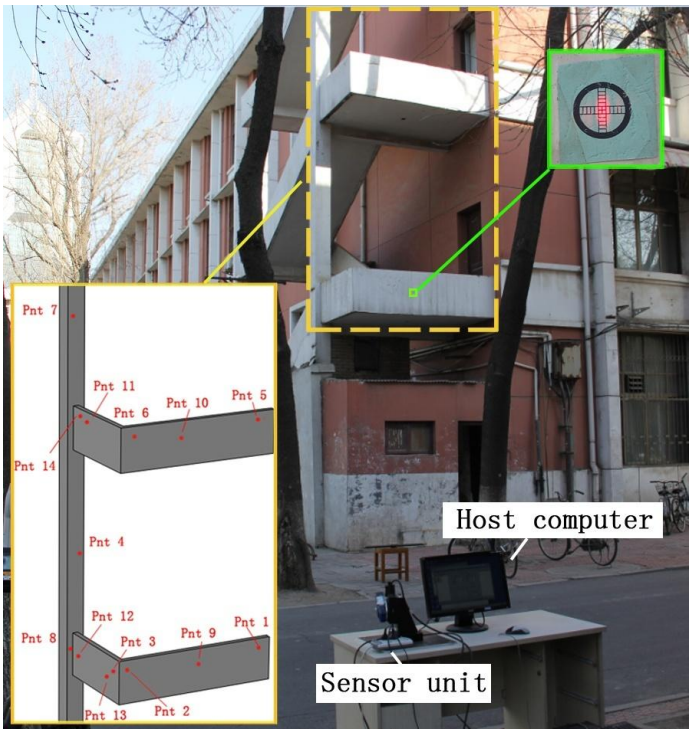

Figure.9 Outdoor experiment condition

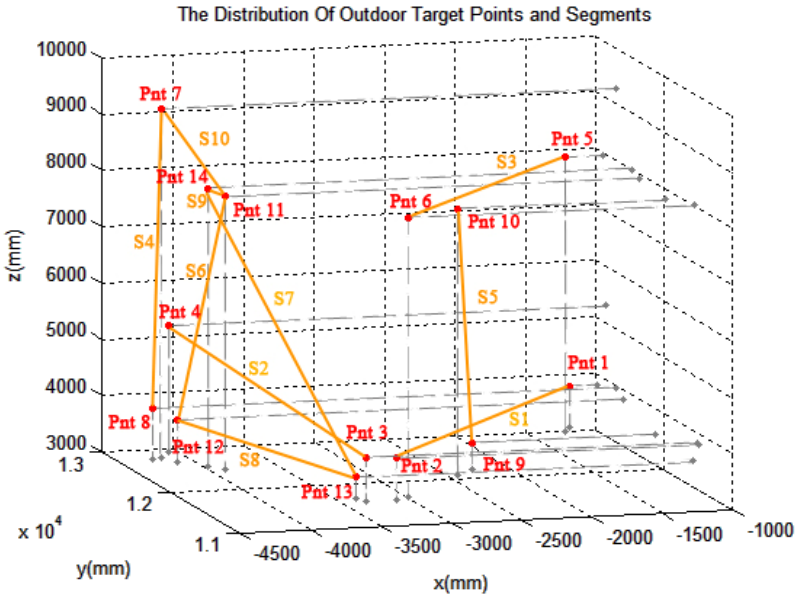

Figure.10 The distribution of outdoor target points and segments

The general performance of the outdoor experiment is not as good as the indoor ones, due to the large pitching angle. The last three segments (S8, S9, S10 in Figure 10) show the largest deviations. The main reason is their locations. We can observe from Figure 9 that the associated points of these segments are all located on the left side wall of the building. A sharp angle between the laser beam and wall exists, which makes it hard to accurately aim at the target point because of the relatively large laser spot (image the laser beam as a cylinder and the area of laser spot is the cross section cut by a very skew plane) under this circumstance. The reflection light for the LRF to measure the distance measurement also becomes weak in this case, which results in a low accurate measurement distance. This assumption can be verified through the Segment 3 as well. Although

both Segment 1 and 3 located in the front side of the building which means a relatively large horizontal intersection angle between the laser beam and target plane, the Segment 3 lies on a higher place than Segment 1, which leads to a sharper vertical intersection angle between the laser beam and the target plane (see the vertical angles of point 1, point 2, point 5, and point 6. The larger the vertical angles are, the sharper the intersection angles are). The larger deviation is observed from Segment 3. This experiment result suggests the importance of a good deployment of the proposed system. For the large-scale measurement task, a deployment location that faces to the target points with relatively large horizontal and vertical intersection angles is preferred. The detailed system uncertainty analysis can be found in [26].

5. Conclusion

A prototype of a novel cost-effective, large-volume 3D measurement system has been assembled and tested. The non-orthogonal structure lowers the manufacture time and economic cost of the system. Evaluation tests show, with the proposed calculating algorithm and kinematic model, the non-orthogonal system can achieve relevant performance. The measurement accuracies are better than 0.3 mm in the simulation and below 3.5 mm in practice with observation distances of more than 15 m. As more precise rotary tables and laser range finders may be available in future, the potential of the system is promising.

Acknowledgments: This work was funded by the National Natural Science Foundation of China (61771336，61671321，51475328).

References

1. Kyle S. Large-Scale Metrology. Handbook of Measuring System Design. 2005.
2. Fan, Kuang-Chao, Yetai T. Fei, X. F. Yu, Y. J. Chen, Weili L. Wang, F. Chen, and Y. S. Liu. "Development of a low-cost micro-CMM for 3D micro/nano measurements." Measurement Science and Technology 17, no. 3 (2006): 524.
3. Driels, Morris R., and Uday S. Pathre. "Vision-based automatic theodolite for robot calibration." IEEE Transactions on Robotics and Automation 7.3 (1991): 351-360.
4. Psimoulis, Panos A., and Stathis C. Stiros. "Measuring deflections of a short-span railway bridge using a robotic total station." Journal of Bridge Engineering 18.2 (2013): 182-185.
5. Aguado, S., Samper, D., Santolaria, J., & Aguilar, J. J. "Identification strategy of error parameter in volumetric error compensation of machine tool based on laser tracker measurements." International Journal of Machine Tools and Manufacture 53.1 (2012): 160-169.
6. Franceschini, Fiorenzo, and M. Galetto. "Large-scale dimensional metrology (LSDM): from tapes and theodolites to multi-sensor systems." International Journal of Precision Engineering and Manufacturing 15.8(2014):1739-1758.
7. Zhang, Zili, Zhu, Jigui, Zhou, Hu, and Ye, Shenghua. "The guidance methodology of a new automatic guided laser theodolite system." International Conference of Optical Instrument and Technology. International Society for Optics and Photonics, 2008.
8. Muelaner, Jody E., and Paul Maropoulos. "Large scale metrology in aerospace assembly." 5th international conference on digital enterprise technology. University of Bath, 2008.
9. Zhang, Xiaohu, Zhu, Zhaokun, Yun Yunana, and Ou Jianliang. "A universal and flexible theodolite-camera system for making accurate measurements over large volumes." Optics and Lasers in Engineering 50.11 (2012): 1611-1620.
10. Knittel, Ronald A. "Laser theodolite." U.S. Patent No. 4,988,192. 29 Jan. 1991.
11. Lau, Kam C., and Robert J. Hocken. "Three and five axis laser tracking systems." U.S. Patent No. 4,714,339. 22 Dec. 1987.
12. Kavanagh, B. F. and Glenn Bird, S. J. Surveying principles and applications (5th ed.). Prentice Hall. 2000 pp. 256–266.

13. ebay, NEW LEICA TS16R1000 P 3" ROBOTIC TOTAL STATION, accessed Nov.11, 2016 http://www.ebay.com/itm/NEW-LEICA-TS16R1000-P-3-ROBOTIC-TOTAL-STATION-W-POWERSEARCH-1YR-WARRANTY-/231722713644?hash=item35f3c0022c:g:VlgAAOSwNgxWDBgr
14. Lichti, Derek D. "Error modelling, calibration and analysis of an AM–CW terrestrial laser scanner system." ISPRS Journal of Photogrammetry and Remote Sensing 61.5 (2007): 307-324.
15. Du, Jun-Feng, Meng-Wei Zhang, and Xiao-Ming Zhang. "Angle measurement accuracy of photoelectric theodolite." Yingyong Guangxue(Journal of Applied Optics) 33.3 (2012): 466-473.
16. Martin, D., and D. Chetwynd. "Angle calibration of robotic total stations and laser trackers." XIX IMEKO World Congress: Fundamental and Applied Metrology. 2009.
17. Wu B and Yang S, "Research of measurement technology of nonorthogonal shaft laser theodolites", Laser Technology, 2015 Jul 14,39(5): 603–609 (in Chinese)
18. Wu. B and Xie S, "Correction of the sight axis parameters for non-orthogonal laser theodolite", Journal of Optoelectronics • laser, 2015 Sept, 26(9): 1700-1706 (in Chinese)
19. Wu, Bin, Yang, Fengting, Ding, Wen, and Xue, Ting. "A novel calibration method for non-orthogonal shaft laser theodolite measurement system." Review of Scientific Instruments 87.3 (2016): 035102.
20. Cosser, E., Roberts, G. W., Meng, X., Dodson, A. H., Cosser, E., and Dodson, A. H. "Measuring the dynamic deformation of bridges using a total station." Proceeding of the 11th FIG Symposium on Deformation Measurements, Santorini, Greece. 2003.
21. Gunel, Banu. "Room shape and size estimation using directional impulse response measurements." Proc. Forum Acusticum Sevilla. 2002.
22. Leica, DISTO™ & Lino, accessed on May 24,2016, http://leica-geosystems.com/products/disto-and-leica-lino
23. Morais, João Pedro, Svetlin Georgiev, and Wolfgang Sprößig. Real quaternionic calculus handbook. Springer Basel, 2014.
24. Ickes BP. "A new method for performing digital control system attitude computations using quaternions". AIAA journal. 1970 Jan.8(1):13-7.
25. Horn, Berthold KP. "Closed-form solution of absolute orientation using unit quaternions." JOSA A 4.4 (1987): 629-642.
26. Wu, B., Ding, W., Yang, F., and Xue, T. The Error Analysis of the Non-orthogonal Total Station Coordinate Measurement System. Acta Metrologica Sinica, 2017, 38(6): 661-666. (In Chinese)
27. Rahman, Mohammad Shaifur, and Ki-Doo Kim. "Indoor location estimation using visible light communication and image sensors." Int. J. Smart Home 7, no. 1 (2013): 99-113.